Three-dimensional band mapping by angle-dependent very-low-energy electron diffraction and photoemission: Methodology and application to Cu

V. N. Strocov* and R. Claessen
Experimentalphysik II, Universität Augsburg, D-86135 Augsburg, Germany

G. Nicolay and S. Hüfner
Fachrichtung Experimentalphysik, Universität des Saarlandes, D-66041 Saarbrücken, Germany

A. Kimura, A. Harasawa, and S. Shin
Institute for Solid State Physics, University of Tokyo, Roppongi, Minato-ku, Tokyo 106-8666, Japan

A. Kakizaki
Institute of Materials Structure Science, High Energy Accelerator Research Organization (KEK), Ibaraki 305-0801, Japan

H. I. Starnberg and P. O. Nilsson
Department of Physics, Chalmers University of Technology and Göteborg University, SE-41296 Göteborg, Sweden

P. Blaha
Institut für Physikalische und Theoretische Chemie, Technische Universität Wien, A-1060 Wien, Austria
(Received 17 November 2000; revised manuscript received 2 February 2001; published 27 April 2001)

A method of band mapping providing full control of the three-dimensional **k** is described in detail. Angle-dependent very-low-energy electron diffraction is applied to determine the photoemission final states along a Brillouin zone symmetry line parallel to the surface; photoemission out of these states is then utilized to map the valence bands in the constant-final-state mode. The method naturally incorporates the non-free-electron and excited-state self-energy effects in the unoccupied band, resulting in an accuracy superior over conventional techniques. Moreover, its intrinsic accuracy is less limited by lifetime broadening. As a practical advantage, the method provides access to a variety of lines in the Brillouin zone using only one crystal surface. We extensively tested the method on Cu. Several new aspects of the electronic structure of this metal are determined, including non-free-electron behavior of unoccupied bands and missing pieces of the valence band.

DOI: 10.1103/PhysRevB.63.205108 PACS number(s): 79.20.Kz, 79.60.−i

I. INTRODUCTION

The electronic band structure $E(\mathbf{k})$ is a key property of crystalline solids. UV angle-resolved photoemission (PE) spectroscopy[1,2] is the method that gives the most detailed information about the band structure $E(\mathbf{k})$ resolved in energy and, in principle, in the three-dimensional wave vector $\mathbf{k}$. This technique inherently involves two electron states: an occupied lower state in the valence band and an unoccupied upper state above the vacuum level E_{vac} (in the following we will refer to the bands above E_{vac} generally as the upper bands, and also as unoccupied or final bands to stress the context in which they appear). Determination of $\mathbf{k}$ is based on its conservation in the photoexcitation in the bulk of the crystal. As the photoelectron passes the surface, the surface-parallel component $\mathbf{k}_{\parallel}$ is conserved and can be determined directly from the vacuum wave vector $\mathbf{K}$. However, the surface-perpendicular component $k_{\perp}$ is distorted and can be controlled only if the $k_{\perp}$ dispersion of one of the two involved electron states in the bulk is known. Commonly, determination of $k_{\perp}$ is based on an empirical free-electron-like (FE-like) model for the upper bands. However, in many cases, especially for systems with highly inhomogeneous electron density, the upper bands demonstrate strong deviations from this model, non-free-electron (non-FE) behavior. To circumvent this problem, several schemes for absolute PE band mapping have been developed, including triangulation.[3] They are all rather ineffective, however, in the sense that a vast amount of experimental spectra has to be processed in order to obtain a few points of $E(\mathbf{k})$.[2]

Only recently has it been demonstrated[4] that the PE upper states may independently be determined by very-low-energy electron diffraction (VLEED), which covers the energy range below ~40 eV typically used for the final-state energies in PE band mapping. This is based on the fact that the PE upper states are related to the LEED states by time reversal.[1,5,6]

The idea of VLEED band determination is clear from the matching approach of the dynamic LEED theory.[7–10] Within this approach the LEED process is described by matching of the vacuum-half-space wave function to the crystal-half-space wave function. The latter is a superposition of the Bloch waves $\Sigma_{\mathbf{k}} T_{\mathbf{k}} \phi_{\mathbf{k}}$ with $\mathbf{k}$ satisfying, by the surface-parallel momentum conservation, the condition $\mathbf{k}_{\parallel} = \mathbf{K}_{\parallel} + \mathbf{g}$ ($\mathbf{g}$ is a surface reciprocal vector). The total elastic reflection $R(E)$, or, more conveniently, elastic transmission $T(E) = 1 - R(E)$, is then connected to the band structure $E(k_{\perp})$ along the surface-perpendicular direction(s) in the Brillouin zone (BZ) defined by $\mathbf{k}_{\parallel} = \mathbf{K}_{\parallel} + \mathbf{g}$. It is important that in the $E(k_{\perp})$ band manifold there are only few bands, which effectively

couple to the incident plane wave and take up significant *partial absorbed currents* $I_{\mathbf{k}}$ into the crystal;[11–14] only these *coupling* bands are effective in the VLEED process. Whenever the electron energy passes a *critical point (CP)* in the $k_\perp$ dispersion of these bands (like the edge of a local band gap formed, for example, on a surface-parallel symmetry line), the associated rapid variation of the wave function causes a rapid change in $T(E)$ signaled by an extremum in dT/dE. Thus the extrema in the VLEED spectrum dT/dE reveal the CP's in the coupling bands. This simple idea enables quantitative experimental determination of the energies of these CP's.[4,11,15] From these characteristic points, the full band dispersions may be recovered: in the surface-perpendicular band structure $E(k_\perp)$ by using the technique of band fitting to the experimental CP's,[4,12] and in the surface-parallel $E(\mathbf{k}_\parallel)$ by direct band mapping of the CP's as a function of $\mathbf{K}_\parallel$,[15,16] as illustrated in more detail here.

Implications of VLEED in PE band mapping use the fact that the PE final states, implying the sudden approximation,[17] are the time-reversed LEED states. Moreover, the partial photocurrents from the upper bands, constituting the PE final state, are proportional to the currents $I_{\mathbf{k}}$ absorbed by these bands in VLEED.[5,12,13] Therefore, the coupling bands found in the VLEED experiment can be used as the dominant final bands in PE mapping of the valence band. As this combined VLEED-PE approach employs the true upper bands not restricted to the FE-like approximations and incorporating the excited-state self-energy effects, it provides superior accuracy and, in the sense of controlling the three-dimensional $\mathbf{k}$, an *absolute* band mapping.[4] Its additional advantage is the possibility of using low photon energies $h\nu$, where the FE approximation is generally inappropriate, to achieve maximal escape-length-limited $k_\perp$ resolution and instrumentally limited $\mathbf{k}_\parallel$ resolutions.

VLEED-PE band mapping can be based either on the VLEED band fitting in $E(k_\perp)$ or on the direct band mapping in $E(\mathbf{k}_\parallel)$. The first method has recently been realized and applied to layered materials with strong non-FE behavior of the upper bands, and provided consistent resolution of their layer-perpendicular $E(\mathbf{k})$.[4,18] Although the accuracy of this method is in practice sufficient, its flaw is the use of a fitting procedure. In contrast, the second method should be direct and more accurate. We here present its realization as the angle-dependent *VLEED-constant-final-state PE (VLEED-CFSPE)* method.

The idea of the VLEED-CFSPE method is simple. Angle-dependent VLEED is first applied to determine the upper band gaps whose $\mathbf{k}$ is located on a symmetry line parallel to the surface; PE out of these gaps, employing the CFS mode, is then utilized to directly map the valence bands along this line. The method inherits thus the ideas of band-gap PE.[19] In contrast to the conventional PE band mapping procedure [employing the energy distribution curve (EDC) mode in the normal emission geometry and varying the photon energy $h\nu$], our method (1) utilizes *off-normal* PE data; (2) does not depend on the strength of the non-FE effects but rather utilizes them.

This work presents application of the VLEED-CFSPE method to Cu. We have chosen this material with well-documented[20–23] $E(\mathbf{k})$ in order to test the method exhaustively, although the method is most effective for non-FE materials. A brief account of this work has been published earlier;[24] now we focus on the technical details and properties of the method. We also report on the non-FE behavior of upper bands of Cu, which, contrary to the common belief, is significant in certain regions. A separate paper[25] presents an intriguing comparison of the upper and valence band $E(\mathbf{k})$ to a state-of-the-art density functional theory (DFT) band calculation, which reveals profound self-energy effects despite the less correlated nature of Cu.

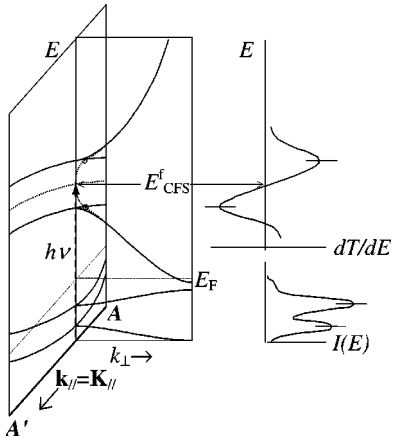

FIG. 1. The idea of the angle-dependent VLEED-CFSPE method: AA' is a surface-parallel symmetry line. The upper bands smoothed by the electron absorption are shown dotted with their CP's indicated by circles. The final-state energies E^f_{CFS} locate $k_\perp$ on the AA' line, and the CFS PE spectra as a function of $\mathbf{k}_\parallel$ directly yield the valence band $E(\mathbf{k})$ along this line.

II. IDEA

The angle-dependent VLEED-CFSPE method uses the upper bands determined by VLEED to guide the PE experiment. The idea of the method is illustrated in Fig. 1. Let AA' be a surface-parallel symmetry line whose $k_\perp$ is constant.

First, one proceeds with an angle-dependent VLEED experiment to determine the upper bands along the AA' line. For any incident $\mathbf{K}_\parallel$, the states excited in the solid lie along a surface-perpendicular direction whose $\mathbf{k}_\parallel$ is constant and determined by the parallel momentum conservation $\mathbf{k}_\parallel=\mathbf{K}_\parallel+\mathbf{g}$. The VLEED spectrum reflects the corresponding $E(k_\perp)$. As the $\mathbf{k}_\parallel=\mathbf{K}_\parallel+\mathbf{g}$ direction is perpendicular to the symmetry line AA', the bands in $E(k_\perp)$ have on AA' extrema of their dispersion, which are the CP's forming the local band gaps. If these bands couple to the incident plane wave, the CP's show characteristic minimum-maximum structures in the VLEED spectrum dT/dE, which reflect crossing of the AA' line with well-defined $k_\perp$. Mapping the energies of the experimental dT/dE extrema as a function of $\mathbf{k}_\parallel$ produces a pair of upper bands along AA' with $\mathbf{k}$ fixed three-dimensionally: $k_\perp$ is fixed on AA', and $\mathbf{k}_\parallel$ is defined by the parallel momentum conservation. Now this picture should be extended to include the electron absorption, characterized by

the potential $V_i \neq 0$, in the VLEED excited state. The absorption results in damping of the excited-state Bloch waves described by complex $k_\perp$. The band dispersions on $\mathrm{Re}\, k_\perp$ become smooth and go continuously through the band gaps,[9,26] as shown in Fig. 1. Their CP's do not disappear, however, they become the points of extremal (inverse) band curvature[11] slightly shifted in $k_\perp$. The excited-state bands intersect the symmetry line AA' at an energy nearly halfway between the CP's reflected by the dT/dE extrema. Mapping this energy as a function of $\mathbf{k}_\parallel$ produces the experimental excited-state upper band along the AA' line with well-defined $\mathbf{k}$.

Second, the valence bands are determined using angle-dependent PE measurements in the CFS mode. The final-state energies $E^{\mathrm{f}}_{\mathrm{CFS}}$ are varied as a function of the photoelectron $\mathbf{K}_\parallel$ to follow the VLEED-determined excited-state upper band along the AA' line. $\mathbf{k}$ thus remains fixed on AA', and plotting the PE intensity as a function of $\mathbf{k}_\parallel$ produces a direct image of the valence bands along this surface-parallel symmetry line with $\mathbf{k}$ fixed three dimensionally.

Note that, while the conventional band mapping method employs scanning in $k_\perp$, the VLEED-CFSPE method scans in $\mathbf{k}_\parallel$. It probes the valence band in an extremum of $E(k_\perp)$, i.e., at a point of maximal one-dimensional density of states (1DOS) $\partial k_\perp / \partial E$, which results in an intensity gain.

III. EXPERIMENTAL PROCEDURE AND RESULTS

A. Experimental geometry

Efficient application of the VLEED-CFSPE method assumes optimization of the experimental geometry according to the crystallographic structure. For fcc materials use of the (110) surface is optimal: Fig. 2(a) shows the fcc bulk BZ with the inserted (110) surface BZ. Clearly, this surface should give access to the whole surface-parallel symmetry plane $\Gamma KLUX$.

The correspondence of the azimuths in the (110) surface BZ to the symmetry lines in the bulk BZ is somewhat complicated because the surface-parallel momentum conservation invokes, in addition to the $\mathbf{k}_\parallel = \mathbf{K}_\parallel$ *direct* line, also the $\mathbf{k}_\parallel = \mathbf{K}_\parallel + \mathbf{g}$ lines with $\mathbf{g} \neq \mathbf{0}$ (referred to as surface *umklapp* lines). For example, the normal incidence (emission) $\mathbf{K}_\parallel = \mathbf{0}$ corresponds to the $\mathbf{k}_\parallel = \mathbf{0}$ direct line ΓK and the $\mathbf{k}_\parallel = \pm \mathbf{g}_{\overline{2\Gamma Y}}$ umklapp lines XU in the reduced BZ. With the umklapp lines, the correspondence may be seen most clearly using a repeated-zone scheme as shown in Fig. 2(b). Variations of $\mathbf{K}_\parallel$ in the three main azimuths are schematically shown as a group of three corresponding vectors, which is translated through the repeated surface BZ's according to all $\mathbf{g}$. Consider now the reduced bulk BZ and, specifically, its surface-parallel $\Gamma KLUX$ plane. Upon variation of $\mathbf{K}_\parallel$, the corresponding variations of the reduced $\mathbf{k}_\parallel$ take place along several parallel lines, with $\mathbf{k}_\parallel$ coming into and leaving the $\Gamma KLUX$ plane in the reduced BZ. Then the variations of $\mathbf{K}_\parallel$ in the $\overline{\Gamma Y}$ azimuth of the surface BZ project onto the ΓX line in the bulk BZ (in fact, to the two equivalent lines $\overline{\Gamma}$ to X, and X to Γ), in ΓX to ΓK and XU lines, and in $\overline{\Gamma S}$ to ΓS and XL.

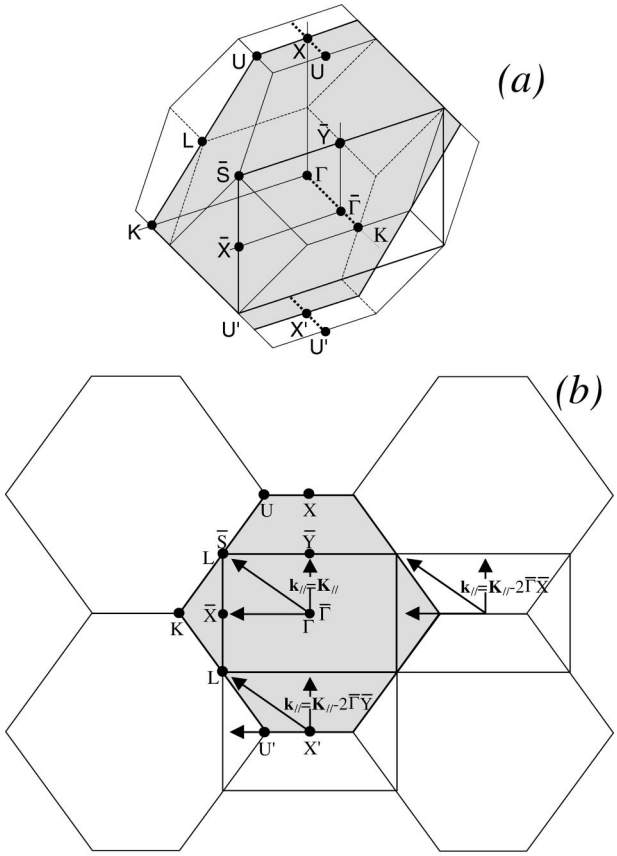

FIG. 2. Geometry of a VLEED CFS experiment on a fcc (110) surface: (a) the bulk BZ with the surface BZ inserted; the surface-parallel symmetry plane $\Gamma KLUX$ shown by shading. (b) Variations of $\mathbf{K}_\parallel$ in the surface BZ projected onto variations of $\mathbf{k}_\parallel$ in the $\Gamma KLUX$ plane of the bulk BZ using the repeated-zone scheme.

An important issue is the energy of the band gaps used in the VLEED-CFSPE experiment, which should fit the available photon energy range. Suitable band gaps are not only located on a surface-parallel symmetry line, but also should be formed by the bands coupling to the vacuum plane wave and thus be effective in the VLEED and PE processes. A rough estimate of their energy can be obtained using a qualitative analysis of the corresponding wave functions taken from any band calculation,[14] or even using the FE approximation (in the reduced-zone scheme, the coupling bands correspond in this case to a single plane wave with $\mathbf{k}_\parallel + \mathbf{G}_\parallel = \mathbf{K}_\parallel$). For Cu, suitable band gaps for the ΓX, ΓKXU, and XL lines lie in the range of $\sim$15 to 30 eV (here and throughout the paper the energies are relative to E_F). These energies ideally fit standard grazing-incidence UV monochromators, and are sufficiently low to provide good intrinsic $k_\perp$ resolution (see below). For the ΓL line they rise above $\sim$50 eV, which is less suitable as the $k_\perp$ resolution becomes worse.

Other fcc surfaces may also be used, although less effectively. The (100) surface geometrically allows one to probe the whole ΓXWK symmetry plane and the XUW rectangles. However, for ΓXWK the suitable band gaps are above $\sim$40 eV (moreover, near $\mathbf{K}_\parallel = 0$ there will be a complication due to a doublet composition of the coupling bands[12]). For

XUW these band gaps are just above E_{vac}, which is less convenient experimentally. The (111) surface allows access to all $LKWU$ hexagons at energies above ~ 60 eV, which is less suitable due to degrading of the $k_\perp$ resolution, and the ΓK symmetry line in a convenient range from 25 to 45 eV.

B. Unoccupied $E(\mathbf{k})$ by VLEED

1. Experimental technique

The VLEED experiment was performed with a standard four-grid LEED unit. To achieve the lowest primary energies, the retarding field mode was used.[27–29] Briefly, the voltages on the electrodes of the gun relative to the cathode are kept as required to maintain optimal focusing of the beam (normally from $+100$ to $+300$ eV). With the sample kept at ground potential, the electrons are decelerated in a retarding field between the gun and the sample to the low primary energies E determined by the cathode bias relative to the ground. This mode enables optimal and constant-current operation of the gun down to zero energies. Moreover, the electron energy being sufficiently large over the major part of the trajectory reduces the influence of stray magnetic fields (although their compensation using Helmholtz coils is useful). Focusing of the electron beam was controlled by observing the reflected beams on the screen.

The main experimental difficulty associated with the retarding field mode is that if the sample is rotated for off-symmetry measurements the arising asymmetry of the retarding field deviates the electron trajectories depending on energy E and sample rotation angle α (which now differs from the incidence angle). Tight control over the electron trajectories is required, however, to obtain reliable VLEED data, especially concerning $\mathbf{K}_\parallel$, which determines the probed surface-perpendicular direction in the bulk BZ. Based on an extensive electrostatic ray-tracing analysis, effective measures to overcome this difficulty have recently been found.[29] (1) It was shown that due to the retarding field the $\mathbf{K}_\parallel$ dependence on E and α becomes close to bilinear and can be accurately parametrized by a biquadratic function $K_\parallel(E,\alpha) = \Sigma_{l,m=0}^{2} A_{lm} E^l \alpha^m$ with the residual error equivalent to the sample rotation of only $\sim 0.3°$. This allows one to determine $\mathbf{K}_\parallel$ empirically by using the parametrized dependence with the coefficients A_{lm} fitted to some characteristic experimental points and diffraction patterns. This approach not only saves time over an explicit determination of $\mathbf{K}_\parallel$ in ray-tracing calculations, but in practice turns out even more accurate because it takes into account to some extent the stray magnetic and electrostatic field effects. (2) It was shown that the beam displacement over the sample shows, apart from the energy dependence, an almost linear increase with increasing α. This allows one to compensate this increase and reduce the displacement below ± 1 mm by an offset of the sample surface from the manipulator rotation axis outward by ~ 3 mm.

Of other practical matters, it should be noted that the retarding field makes the electron trajectories extremely susceptible to asymmetries of the experimental geometry. This requires use of a symmetric sample holder and careful centering of the electron beam. An asymmetry introduced by the massive manipulator parts above the sample should be compensated by attaching a symmetric metal shield below the sample. Further details are discussed in Ref. 29.

The VLEED experiment should give the elastic electron transmission $T(E)$, which in principle is obtained from measurements of the elastic reflectivity as $T(E)=1-R(E)$. However, in practice $T(E)$ may be replaced by the total transmission, as its inelastic component depends smoothly on energy. This allows measurement of $T(E)$ from the current absorbed by the sample. This technique is commonly referred to as target (or total) current spectroscopy (TCS) (see, e.g., Ref. 28). To reduce the ripple in the target current signal, we used a current-input preamplifier mounted near the feedthrough to the sample. It should be noted that the TCS technique benefits from excellent signal/noise ratio, which allows for a data acquisition time of less than 1 min per spectrum.

The Cu(110) sample was electropolished and cleaned *in situ* by standard Ar sputtering and annealing cycles. Besides a bright LEED pattern, the excellent quality of the surface was confirmed by observation of surface resonances (see below).

2. VLEED experimental results

The experimental angle-dependent VLEED data were smoothed by a Gaussian with the 0.25 eV half width at half maximum (HWHM) ($\sim$ the primary beam energy spread) to reduce the noise, and rendered into the dT/dE spectra shown in Fig. 3. As discussed above, this representation reveals the band structure information most directly: the dT/dE extrema reflect the CP's in the $k_\perp$ dispersion of the bands coupling to vacuum (except for weaker surface resonance structures also seen in Fig. 3).[30,31] Representation of the VLEED data in the negative second derivative $-d^2T/d^2E$, often used by analogy with PE, is less appropriate: the $-d^2T/d^2E$ peaks are considerably shifted from the CP's toward the band interior, and spurious structures in the band interiors are generated. Note that, while in PE spectra the band structure information is displayed by their maxima, in the VLEED spectra it is contained in both the maxima and minima of dT/dE. The structures are generally more asymmetric, and identification of their energies using the second derivative is less accurate.

The whole body of the VLEED data were further rendered into a $\mathbf{K}_\parallel$ *dispersion map* of the dT/dE spectra shown in Fig. 4. The shading in this map shows the spectral regions from the dT/dE maxima to the nearest minima higher in energy, which are identified by $(d/dE)(dT/dE)<0$. The positions of the extrema themselves are shown by bars. The amplitude and sharpness of the extrema, determining the accuracy of their position, are shown as $|(d^2/dE^2)(dT/dE)|$ in a gray scale.

The experimental $\mathbf{K}_\parallel$ dispersion map of the dT/dE spectra is basically a direct *image of the surface-projected* $E(\mathbf{k})$ of the unoccupied bands (except for the bands with insignificant coupling to vacuum).[31] Indeed, the shading shows the interiors of the coupling bands surface-projected out of $E(k_\perp)$ along the $\mathbf{k}_\parallel = \mathbf{K}_\parallel + \mathbf{g}$ lines in the bulk BZ, and the

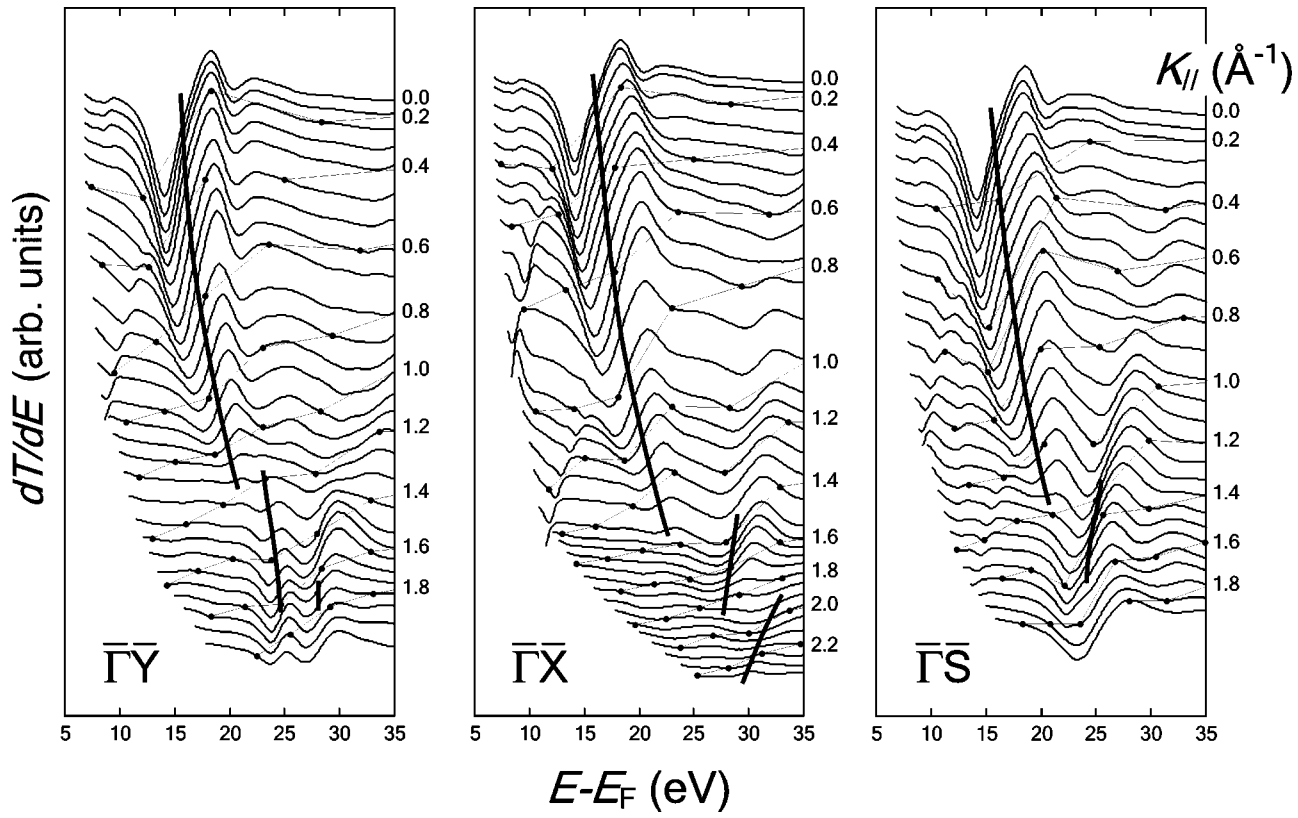

FIG. 3. Experimental VLEED spectra of dT/dE in the indicated azimuths of the surface BZ: The sample rotation (which differs from the true incidence angle) increments in steps of 1°. Thin broken lines show the points of the indicated constant $K_\parallel$ values (the $K_\parallel$ determination accuracy, limited by the rms errors of the biquadratic parametrization and of the fitting procedure, is ~ 0.04 Å^{-1}). The spectra are clipped up to 2 eV from the primary dT/dE peak (onset of the target current at $E_{\rm vac}+\hbar^2K_\parallel^2/2m$). The bold lines show the minimum-maximum structures corresponding to the band gaps in the ΓXWK symmetry plane used in the CFS PE experiment (see the text below).

points are the CP's of these bands. We stress that our data processing is fully automatic, which provides the physical information most objectively.

It should be noted that VLEED spectroscopy, like any other spectroscopy, has a certain *intrinsic accuracy*.[18] It is characterized by intrinsic shifts of dT/dE extrema from the true CP's due to smooth variations of $T(E)$ within the band, distorting influence of the surface barrier, and, mainly, overlap of the spectral structures. These shifts are normally within 0.1–0.3 eV. Relative to the bandwidth, this is of the same order as in PE spectroscopy (see below). Depending on broadening of the spectral structures, the shifts are minimal at the lowest energies due to small V_i. In principle, the intrinsic accuracy influence may be reduced using corrections found from a model calculation.[15,25]

C. VLEED data analysis: the CFS energies

The VLEED spectra were further interpreted to identify the extrema corresponding to the $\Gamma KLUX$ surface-parallel symmetry plane, and from them determine the final-state energies $E_{\rm CFS}$ for the following PE experiment. The interpretation employed *reference* band calculations, focusing on the band configuration and coupling properties characterized by partial absorbed currents $I_{\mathbf{k}}$, to link the dT/dE extrema with particular CP's in $E(\mathbf{k})$.

Such reference calculations can be qualitative and use various time-saving approximations. We here used the following simplifications: (1) *No-absorption (NA) approximation.*[11] Damping of the Bloch waves due to V_i results in smoothing of the band $k_\perp$ dispersions with the CP's becoming the extremal points of the inverse band curvature. As these points are only slightly displaced from the CP's in the undamped ($V_i=0$) bands (see Fig. 1), the VLEED spectral structures can in fact be related to the undamped $E(\mathbf{k})$. This approximation holds as long as V_i remains smaller than or at least comparable with the energy separation between the CP's, which is mostly the case at the VLEED energies; (2) *Infinite-crystal approximation.* Even if $V_i=0$, description of the VLEED process should in principle include, in addition to the propagating bulk Bloch waves, the surface ones which are damped by scattering off the crystal potential. This requires finding the corresponding complex $E(\mathbf{k})$ by solving the secular equation on the complex $k_\perp$, which computationally is very hard.[8,32,33] However, the VLEED spectral structure is formed predominantly by the bulk Bloch waves. This fact allows one to describe the VLEED process qualitatively based on the bulk crystal $E(\mathbf{k})$. Use of these two approximations enables one to exclude complex $k_\perp$ and reduce the reference calculations essentially to nominal bulk band calculations employing simple diagonalization of a real symmetric Hamiltonian matrix.

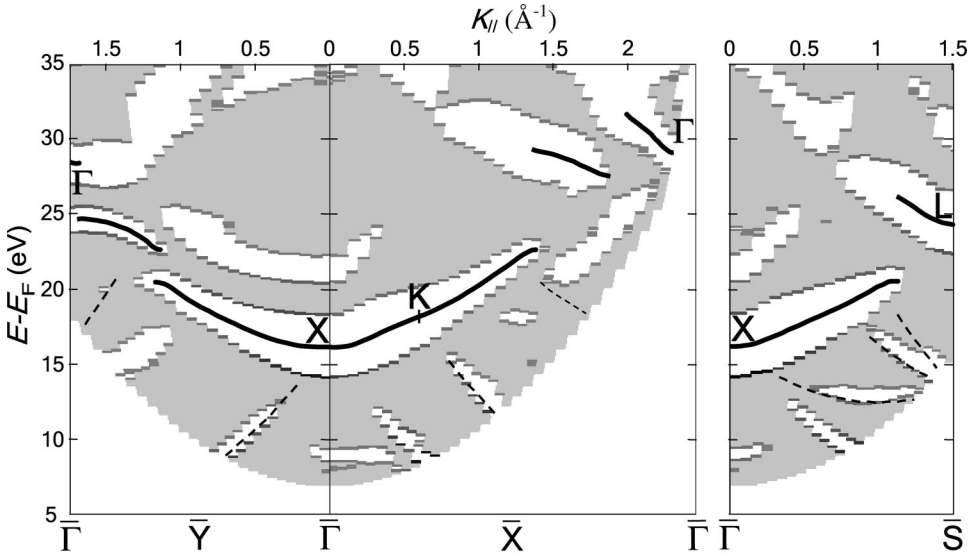

FIG. 4. $\mathbf{K}_\parallel$ dispersion map of the experimental VLEED spectra: The shading fills the maxima-to-minima areas in the dT/dE spectra, and the bars show the positions of the extrema themselves. Physically, this map is the surface-projected dispersion $E(\mathbf{k}_\parallel)$ of the coupling bands: the shading shows the interiors of these bands framed by the CP's. The extrema are shown in a gray scale according to $|(d^2/dE^2) \times (dT/dE)|$ ($\sim$ their amplitude $\times$ sharpness). The region below $E_{\rm vac}+\hbar^2K_\parallel^2/2m+2$ eV is clipped as in Fig. 3. The dotted lines show the diffraction beam thresholds $E_{\mathbf{g}}=(\hbar^2/2m)(\mathbf{K}_\parallel+\mathbf{g})^2$ in the low-energy part of the spectra, where the surface resonance structures may exist (see the text below). The bold lines show the final-state energies used in the PE experiment with the corresponding directions in the bulk BZ indicated.

We realized the reference calculations using the empirical pseudopotential method (EPM) with a minimal basis set of 27 plane waves to calculate $E(\mathbf{k})$. [Other band calculation methods may also be used: for example, later[34] we employed the first-principles full potential linearized augmented plane wave (FLAPW) code WIEN97.[35]] The pseudopotential Fourier components were adjusted to reproduce roughly a few representative VLEED spectra, including the normal incidence one. To calculate the band partial currents $I_{\mathbf{k}}=|T_{\mathbf{k}}|^2 v_{\mathbf{k}\perp}$, where $T_{\mathbf{k}}$ is the Bloch wave excitation amplitude and $v_{\mathbf{k}\perp}=\partial E/\partial k_\perp$ its surface-perpendicular group velocity, we used the coupling Fourier component–group velocity approximation[13] with the wave functions generated as a by-product of the band calculations. It relates $I_{\mathbf{k}}$ to (1) the partial content of the coupling (incidence-wave-like) Fourier components and (2) $v_{\mathbf{k}\perp}$ of the Bloch waves, using an empirical formula, in a simplified form,

$$I_{\mathbf{k}} \propto \left(\sum_{\mathbf{G}:\mathbf{k}_\parallel+\mathbf{G}_\parallel=\mathbf{K}_\parallel} C_{\mathbf{G}}^2 \right)^{\alpha} (v_{\mathbf{k}\perp})^{\beta}$$

with the coefficients α and β adjusted to model matching calculations (see Ref. 13 for details, including the implementation). This approximation, although sacrificing some amplitude accuracy, is by a factor of $\sim$30 faster and inherently numerically stable compared to the matching. Other bulk crystal approximations[33,36] may also be used.

The interpretation of the VLEED data using the reference calculations is illustrated in Fig. 5. The normal incidence $\mathbf{K}_\parallel=0$ corresponds to the direct line ΓK and the $\mathbf{g}_{2\overline{\Gamma Y}}$ umklapp line UX (see Fig. 2). The extrema in the experimental spectrum are all identified with the CP's in the coupling bands (large $I_{\mathbf{k}}$) of the reference $E(\mathbf{k})$, including a smooth-type CP near 20 eV as a band curvature extremum. Some energy displacements, which are due to the approximate pseudopotential, do not affect the interpretation. There are three CP's placed in the $\Gamma KLUX$ plane, specifically, at the X point (the spectral structures corresponding to the symmetry lines are in fact not necessarily the strongest). If the surface effects are now taken into account, the band gaps will be bridged by real lines of the complex $E(\mathrm{Re}\, k_\perp)$.[9,11,26] With this band configuration they will be passing the X point only between the band extrema of the opposite curvature sign, i.e., between the lowest two CP's. Taking into account the smoothing effect of V_i (see Fig. 1), the excited-state bands will pass this point at the energy halfway between them. This fixes the final-state energy for the PE experiment $E_{\rm CFS}$, which locates $\mathbf{k}$ at the X point. As an off-normal case, Fig. 5 also illustrates the interpretation for $\mathbf{K}_\parallel=2\overline{\Gamma Y}$ (the center of the second surface BZ; see Fig. 2). This particular case corresponds to UX as the direct line and ΓK as the $\mathbf{g}_{2\overline{\Gamma Y}}$ umklapp line, the same as for normal incidence. While in the off-symmetry case $\mathbf{K}_\parallel$ depends on energy, here for simplicity we show one experimental spectrum whose $\mathbf{K}_\parallel$ reaches $2\overline{\Gamma Y}$ near the spectral structure corresponding to the $\Gamma KLUX$ plane (though the $\mathbf{K}_\parallel$ dispersion in this region is rather weak). The choice of $E_{\rm CFS}$ is again evident. Now it locates $\mathbf{k}$ at the Γ point. By virtue of the swiftness of our reference calculations, a similar interpretation was performed readily for the whole body of angle-dependent VLEED spectra.[37] In the investigated energy range $E_{\rm CFS}$ always locates $\mathbf{k}$ on the umklapp line (see Fig. 2).

In addition, we have performed explicit reference calcu-

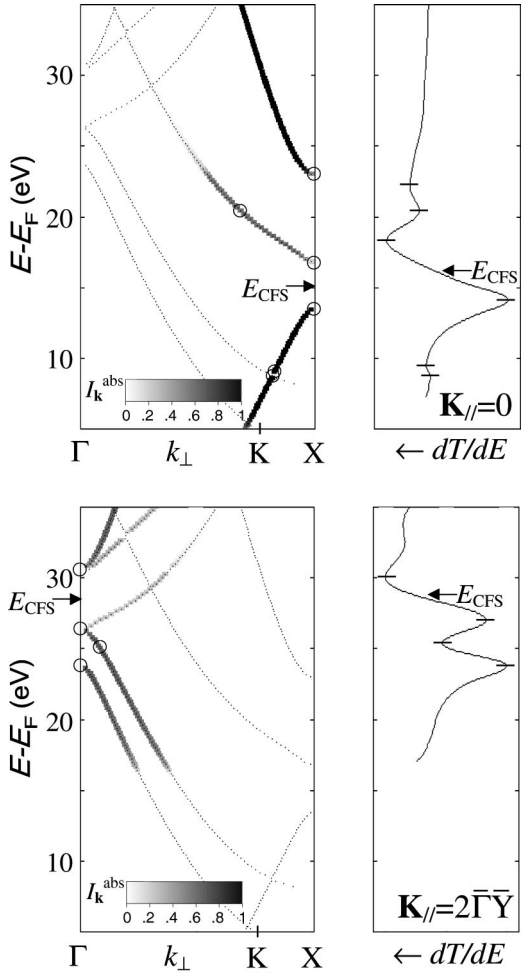

FIG. 5. Interpretation of the VLEED spectra using the reference calculations based on the bulk band structure: Identification of the dT/dE extrema with the CP's in the coupling bands (large $I_{\mathbf{k}}$ shown by gray scale) is evident. This fixes the final-state energies E_{CFS} for the PE experiment, which locates $\mathbf{k}$ in the $\Gamma KLUX$ plane. In the $\mathbf{K}_{\parallel}=2\overline{\Gamma Y}$ case, the shown experimental spectrum is characterized by $\mathbf{K}_{\parallel}$ varying within some $\pm 10\%$ and equal to $2\overline{\Gamma Y}$ near 25 eV.

lations (based on the semi-infinite crystal approach and including V_i) for a few $\mathbf{K}_{\parallel}$ values to check the configuration of the excited-state bands as well as for further use in PE. The corresponding complex $E(\mathbf{k})$ was calculated within the same EPM scheme with a realistic V_i taken as $V_i=0.065(E-E_{\mathrm{F}})$.[38] Such calculations are relatively simple, as locality of the pseudopotential allows one to reduce the secular equation to a simple eigenvalue problem for a complex non-Hermitian matrix[8,32] (other band calculation schemes involve much larger computational problems, and often employ a local EPM fit[8] or the $\mathbf{k}\cdot\mathbf{p}$ expansion[33]). The partial currents $I_{\mathbf{k}}$, which in the picture including V_i are formed by electron capture from the coherent Bloch waves and determined as $I_{\mathbf{k}}=V_i\int(T_{\mathbf{k}}\phi_{\mathbf{k}})^{*}T_{\mathbf{k}}\phi_{\mathbf{k}}d\mathbf{r}$ with the integration in the crystal half space,[12] were calculated from the amplitudes $T_{\mathbf{k}}$ determined by matching (see Refs. 11 and 12 for details). The calculated results are shown in Fig. 6. The coupling

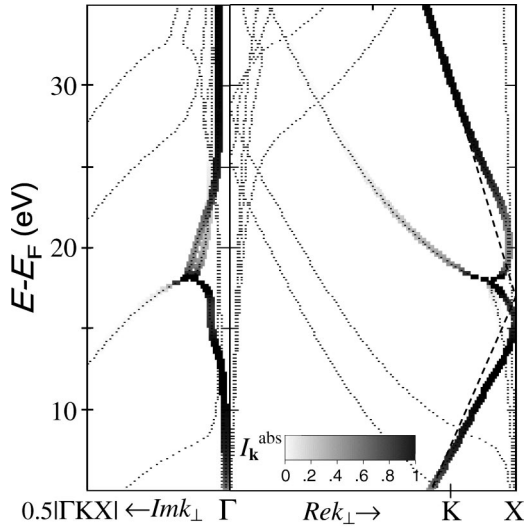

FIG. 6. Reference calculations, based on the semi-infinite crystal picture and including V_i, for the normal incidence case: The band configuration confirms the choice of E_{CFS} in Fig. 5.

bands intersect the $\Gamma KLUX$ plane in the expected band gap, and the energy of the intersection point falls almost in the middle between the two CP's as the band curvature extrema reflected by the VLEED spectral structures (possible displacements are too small to affect the accuracy of the PE experiment). This confirms the above choice of E_{CFS}. Note some increase of $\mathrm{Im}\,k_{\perp}$ in the band gap, which reflects stronger damping of the Bloch waves by elastic scattering off the crystal potential.

The $\mathbf{K}_{\parallel}$ dispersion of E_{CFS} determined for the whole body of the experimental spectra is shown in the VLEED dispersion map in Fig. 4. The corresponding symmetry lines in the bulk BZ are also indicated. We stress that for these energies $\mathbf{k}$ is fixed three-dimensionally: in $\mathbf{k}_{\parallel}$ by parallel-momentum conservation (with a particular $\mathbf{g}$), and in $k_{\perp}$ by being located in the surface-parallel $\Gamma KLUX$ plane.

As a general trend seen in Fig. 4, $E_{\mathrm{CFS}}(\mathbf{K}_{\parallel})$ disperses upward upon increase in $K_{\parallel}$. However, the regions of steady dispersion of the corresponding band gap are interrupted by VLEED structures dispersing downward, which correspond to band gaps coming from the BZ interior into the symmetry plane. Upon further increase of $K_{\parallel}$ the first gap sharply changes its dispersion, deviating from the symmetry plane, and closes. Through a discontinuity, $E_{\mathrm{CFS}}(\mathbf{K}_{\parallel})$ moves into the second gap, which can for a while keep the downward dispersion (as in the large-$K_{\parallel}$ region in the $\overline{\Gamma X}$ azimuth). As the excited-state band goes through the discontinuity almost vertically in a manner similar to Fig. 6, the energy changes within its limits result in insignificant $k_{\perp}$ changes (such a behavior is corroborated by the PE data; see below).

D. Occupied $E(\mathbf{k})$ by CFSPE

The PE experiment was performed at the Photon Factory synchrotron radiation facility, Japan, at beamline BL18A equipped with a grazing-incidence monochromator and an

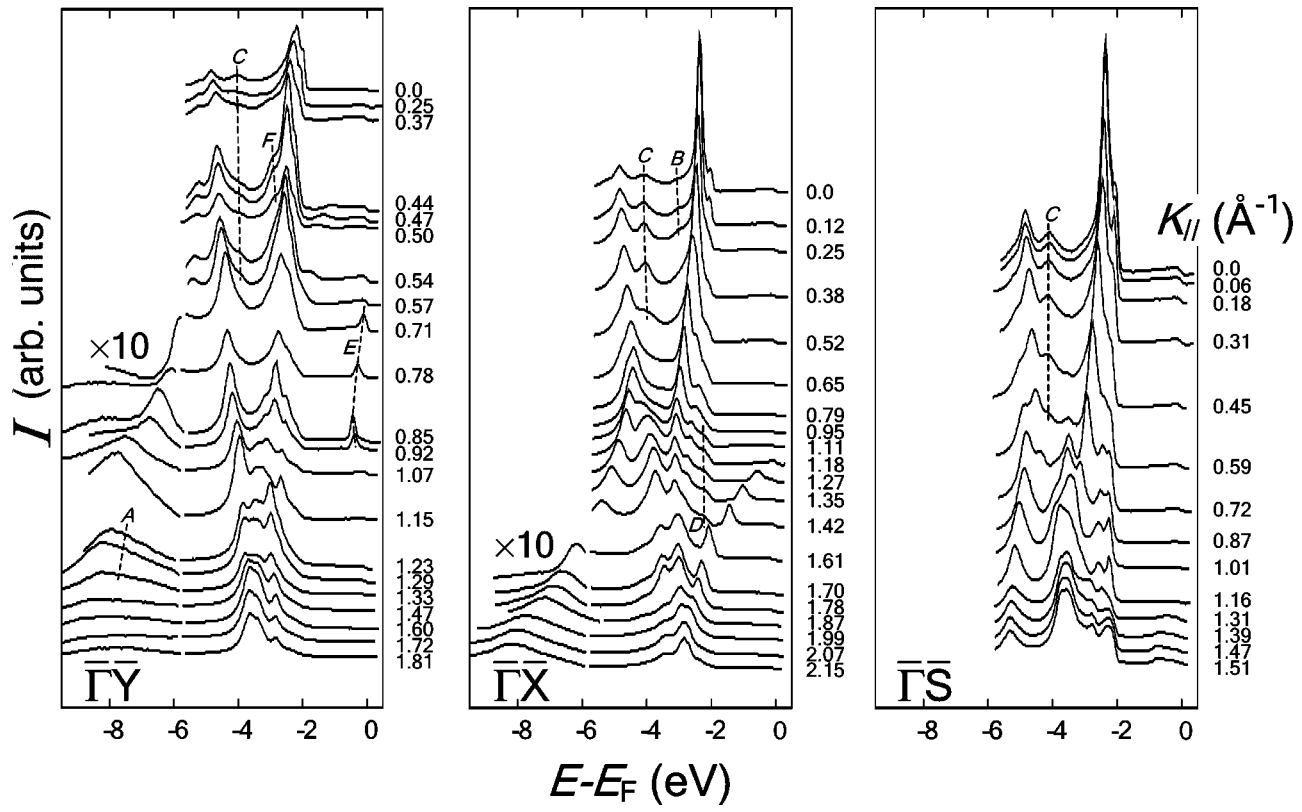

FIG. 7. Experimental angle-dependent CFS spectra; the corresponding $K_{\|}$ values are indicated. The spectra taken below -6 eV are magnified by a factor of 10 and aligned with the higher-energy ones of the same $K_{\|}$.

ADES-500 spectrometer. The photocurrent off the monochromator refocusing mirror was used to normalize the CFS spectra to photon flux. The acceptance angle of the analyzer was 0.5° half width at half maximum. The light incidence angle was set at 45° to provide mixed *s-p* polarization. The high-binding-energy spectra (below -6 eV) were taken in 100 meV steps of the photon energy $h\nu$, and the spectra closer to E_{F} in 50 meV steps. The normal emission angle was adjusted in the EDC mode from the symmetry of the peak energies under analyzer rotation in two perpendicular azimuths. Its setting was accurate within $\pm 0.5°$, and even better in the $\overline{\Gamma Y}$ azimuth where by setting $h\nu$ to 18.6 eV we could follow the highly dispersive *sp* band near E_{F}. The experimental angle-dependent CFS spectra were measured at kinetic energies varying as a function of $\mathbf{K}_{\|}$ according to the E_{CFS} dispersion determined by VLEED, Fig. 4.[39] Note that in the CFS mode every spectrum, taken at a fixed emission angle and kinetic energy, is characterized by constant $\mathbf{K}_{\|}$.

The raw angle-dependent CFS spectra (without noise reduction) are shown in Fig. 7. A spectrum was recorded typically in $\sim$45 min. The major part of the data acquisition time was due to relatively slow setting of the monochromator.

Further data processing was largely similar to that used in VLEED. To reduce the noise, the CFS spectra were smoothed by a Gaussian with the 170 meV HWHM for the low-binding energy spectra and 85 meV for the spectra taken closer to E_{F} (this insignificantly affected resolution of the spectral peaks). Then they were rendered into the negative second derivative $-d^2I/dE^2$ which was thresholded to clip the unphysical negative values and those below a small positive $\varepsilon_{\mathrm{noise}}$ value representing the noise ($\varepsilon_{\mathrm{noise}}$ was taken inversely proportional to the refocusing mirror current used for the normalization). The whole body of these data was further rendered into a $\mathbf{K}_{\|}$ dispersion map, shown in Fig. 8 in a logarithmic gray scale. By virtue of our choice of the final-state energies this map in fact represents the dispersion in the three-dimensional $\mathbf{k}$. We stress that our data processing is fully automatic (the only adjustable parameters were those of the noise reduction, the Gaussian HWHM, and $\varepsilon_{\mathrm{noise}}$, the same for all the processed data) and thus provides most objective information. It is preferred over, for example, evaluation of the peak positions using Lorentzian fitting in which each spectrum should be processed individually and the initial guess for the fitting parameters may influence the results.

The obtained $\mathbf{k}$ dispersion map of $-d^2I/dE^2$ in Fig. 8 is essentially a direct *image of the valence band* $E(\mathbf{k})$ (except for the bands with vanishing matrix element). Indeed, the positions of the $-d^2I/dE^2$ maxima locate the positions of the PE peaks, including the shoulderlike ones, which all reflect the band dispersions (although use of the second derivative implies symmetric peak profiles[23]). Our representation contains in fact more information: the $-d^2I/dE^2$ peak widths characterize the PE peak widths (note that the error bars of the PE peak positions are much smaller than these widths), and the $-d^2I/dE^2$ intensity characterizes the accuracy of the peak location (rather than their intensity, as it

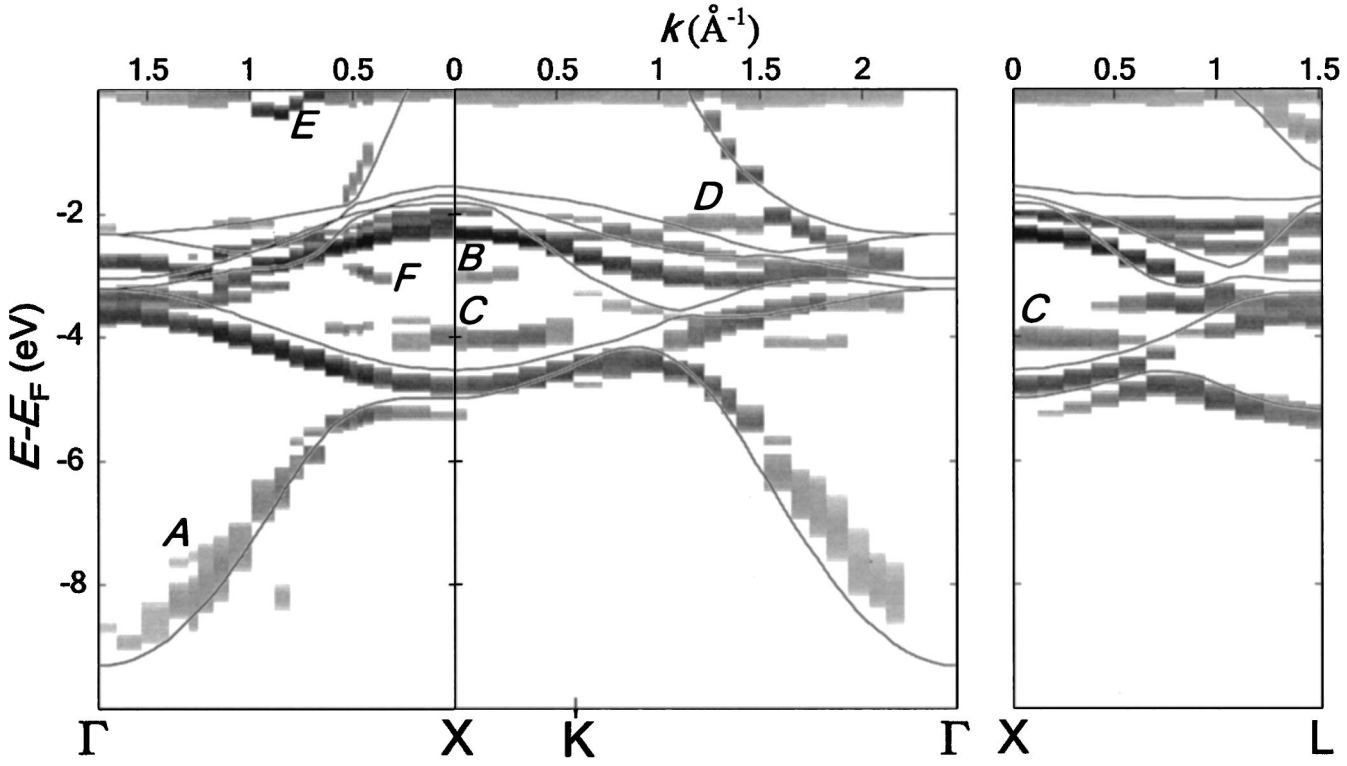

FIG. 8. The **k** dispersion map of the experimental CFS spectra represented as $-d^2I/dE^2>0$. This is essentially a direct image of the valence band $E(\mathbf{k})$. The bands are shifted from the DFT theoretical $E(\mathbf{k})$, shown by thin lines, due to excited-state self-energy effects. The constant line at E_F is due to the Fermi cutoff, and the peaks A–F are spurious structures due to multiple upper band composition, 1DOS maxima, and surface states (see below).

depends also on their sharpness). The valence bands are easily identified by comparison to a DFT band calculation also shown in Fig. 8 [the structures *A*-*F* are not directly connected to the bulk $E(\mathbf{k})$; see below]. This calculation was performed using the FLAPW code[35] WIEN97 and included scalar relativistic effects. The experimental data shows spin-orbit splitting and relativistic matrix element effects.[40,41] Comparison of the experimental $E(\mathbf{k})$ with the DFT picture reveals significant and regular shifts due to the excited-state self-energy effects briefly discussed below.

IV. DISCUSSION

A. Upper bands

1. Role of the coupling properties

The concept of the coupling properties, quantified by the partial currents $I_{\mathbf{k}}$, plays a key role in VLEED data analysis: it enables one to link the spectral structures with particular points in $E(k_\perp)$, even though the latter is usually a multitude of bands. This is clearly seen, for example, in Fig. 5. Only the coupling bands display their CP's as the dT/dE extrema, while all other bands remain ineffective and their CP's invisible. Figure 5 also shows that an estimate of the coupling properties based only on the band dispersion is unreliable: although the coupling bands generally disperse in $k_\perp$ most strongly, the dispersion differences may be too faint to rely on; moreover, in our off-normal case this is misleading. The coupling properties are rather controlled by Fourier composition of the (pseudo) wave functions.[14]

The role of the coupling properties is revealed neatly by comparison of the normal and off-normal cases in Fig. 5 (see also Ref. 16). By the parallel-momentum conservation these two cases correspond, via umklapp, to the same surface-perpendicular lines ΓK and UX (see Fig. 2), and therefore to the same $E(k_\perp)$. Naively, one would expect that the VLEED spectra should also be the same, but they are entirely different. This is because the coupling bands in the same $E(k_\perp)$ changed. Indeed, these bands should have their leading Fourier component $e^{i(\mathbf{k}+\mathbf{G})\cdot\mathbf{r}}$ resemble the incident plane wave $e^{i\mathbf{K}\cdot\mathbf{r}}$ in terms of the surface-parallel components.[14] Then the change of incidence $\mathbf{K}_\parallel$ into the second surface BZ changes this component, and thus the coupling bands. This effect is also obvious in the $\Gamma\bar{Y}$ azimuth of the VLEED dispersion map in Fig. 4: although any two $\mathbf{K}_\parallel$, which are symmetric relative to the $\bar{Y}$ point, correspond to equivalent lines in the bulk BZ, the experimental dispersion has no symmetry.

2. $E(\mathbf{k})$ and the VLEED dispersion map

The $\mathbf{K}_\parallel$ dispersion map of the VLEED spectra as shown in Fig. 4 is essentially the surface-projected dispersion $E(\mathbf{k}_\parallel)$ of the coupling bands (within the intrinsic accuracy). The dispersions of the CP's in this $E(\mathbf{k}_\parallel)$, however, are not equivalent to the entire $E(\mathbf{k})$ along the corresponding surface-

parallel symmetry lines: (1) $E(\mathbf{k}_\parallel)$ shows, in addition to CP's located on these lines, other CP's—those located in the interior of the BZ (strictly speaking, if V_i is taken into account, the CP's associated with the symmetry lines also show a small displacement; see Fig. 1); (2) on the other hand, $E(\mathbf{k}_\parallel)$ misses many bands from $E(\mathbf{k})$ along the symmetry lines—those formed by CP's of the bands in $E(k_\perp)$ that do not couple to vacuum.

Despite the electron absorption, the dispersions in the experimental $E(\mathbf{k}_\parallel)$ are unsmoothed: retaining bands gaps, they are discontinuous functions of energy. At first glance this is surprising, because due to V_i the dispersions in $E(k_\perp)$ become smooth and go through the band gaps continuously (see Fig. 5). In fact, this phenomenon shows interesting physics of the VLEED (and similarly PE) process: V_i results in damping of the wave functions in the surface-perpendicular direction, but parallel to the surface the damping is compensated by surface-parallel invariant excitation by the incident electron beam (whose surface-parallel invariance is limited only by the transverse coherence length). $\mathbf{k}_\parallel$ thus remains real, and $E(\mathbf{k}_\parallel)$ is unsmoothed.

Different effects of V_i on the $k_\perp$ and $\mathbf{k}_\parallel$ dispersions result in different $E(\mathbf{k})$ along the surface-perpendicular and surface-parallel lines connected by symmetry in the bulk BZ (i.e., existence of the surface and V_i break this symmetry). In Fig. 1, for example, even if the $\mathbf{k}_\parallel=\mathbf{K}_\parallel$ line were equivalent by this symmetry to AA', it would not contain the $E_{\mathrm{CFS}}(\mathbf{k})$ band.

3. Surface resonances

The VLEED dispersion map in Fig. 4 shows some spectral structures located near the diffraction beam thresholds $E_{\mathbf{g}}=(\hbar^2/2m)(\mathbf{K}_\parallel+\mathbf{g})^2$ (dashed lines) and not connected with the bulk $E(\mathbf{k})$. They occur due to the surface resonances just below the thresholds as the preemergent beam with $\mathbf{K}_\parallel+\mathbf{g}$ travels parallel to the surface through multiple reflections between the surface barrier and the crystal bulk.[42–44] These structures are superimposed on a weak decrease of the total transmitted current (a dT/dE minimum) above the threshold connected with onset of an additional channel of electron scattering off the crystal.[28]

A popular point of view is that the surface resonances may exist only if supported by a band gap in $E(\mathbf{k})$ that provides effective reflection off the crystal bulk. However, in our data they are located where a strongly coupling band easily transmits electrons into the solid. This seemingly strange effect is because the bands, which couple to the incident plane wave with wave vector $\mathbf{K}_\parallel$, do not couple to and reflect the preemergent beam with $\mathbf{K}_\parallel+\mathbf{g}$.

The resolution of our setup was unfortunately not sufficient to resolve finer details of the surface resonance structures, containing information about the shape of the surface barrier. To our knowledge, we present the first observation of this phenomenon on a loosely packed fcc (110) surface. This is along with the existing observations of image potential states in inverse PE.[45] As the surface resonances are highly sensitive to surface contamination, their existence proves excellent surface quality.

4. Non-FE effects

The VLEED data reveal that the upper bands of Cu contain, contrary to the common belief, significant deviations from the FE-like dispersion in several regions of $\mathbf{k}$ space. This has been noticed in some previous PE studies,[46,47] but only VLEED has allowed us to observe them explicitly. In the following we treat the FE approximation in a generalized sense as an optimal fit of the real $E(\mathbf{k})$ by a parabola $E_{\mathrm{FE}}(\mathbf{k})=(\hbar^2/2m^*)(\mathbf{k}+\mathbf{G})+V_{000}$ with the effective mass m^* and inner potential V_{000} to some extent incorporating the non-FE and self-energy effects. Note, however, that in this approximation among all bands, characterized by different $\mathbf{k}+\mathbf{G}$, only *one* band couples to the vacuum plane wave and thus is effective in VLEED and PE.[14]

In the experimental surface-projected $E(\mathbf{k}_\parallel)$ in Fig. 4 the non-FE dispersion behavior is seen most clearly. The very appearance of CP's in the $k_\perp$ dispersion, reflected by the extrema in the VLEED spectra, is already a non-FE effect. One might nevertheless expect that the dispersion of these CP's would be FE-like. However, dramatic deviations from that are seen in the experimental $E(\mathbf{k}_\parallel)$, in particular closer to the BZ borders: (1) the $\mathbf{k}_\parallel$ dispersions demonstrate large discontinuities where they meet each other and form extended band hybridization regions, often involving many bands (for example, near $K_\parallel=2$ Å^{-1} in the $\overline{\Gamma Y}$ azimuth); (2) although the continuous dispersions are seemingly FE-like, they in fact can be approximated by the FE-like dispersion only *locally* in the sense that the optimal values of V_{000} and m^* will strongly depend on energy and $\mathbf{k}_\parallel$. Correspondingly, the experimental $\mathbf{k}_\parallel$ dispersion of E_{CFS}, which reflects the excited-state $E(\mathbf{k})$ along the chosen lines in the bulk BZ, also shows discontinuities in the extended band hybridization regions near the $\Gamma KLUX$ plane and a nonparabolic behavior. The FE approximation can in fact be reasonable only near the X point and closer to the BZ borders can describe only a general trend. The optimal V_{000} value will be ~ 7 eV, which is about 2 eV above the value estimated in Ref. 20 based on extensive PE data for higher final-state energies (see the comparison in Ref. 24).

In the $k_\perp$ dispersion the non-FE behavior should be less pronounced due to the smoothing effect of V_i. It survives nevertheless in two aspects: (1) The $k_\perp$ dispersion cannot be smoothed into a completely FE dispersion, because the energy width of the band hybridization regions is in general comparable with the V_i values. Moreover, $E(k_\perp)$ may still feature multiple coupling bands (see below). Both effects are clear, for example, near the X point in Fig. 6. They are more pronounced in the extended band hybridization regions seen in $E(\mathbf{k}_\parallel)$; (2) The FE approximation of $E(\mathrm{Re}\,k_\perp)$ will again be only local, with the parameters depending on energy and, as seen in the $E(\mathbf{k}_\parallel)$ plot, $\mathbf{k}_\parallel$. Our observations of the non-FE behavior of upper bands agree with conclusions achieved in a previous attempt at absolute PE band mapping,[46] but there use of a symmetry line at some angle to the surface mixed the effects of V_i on the $k_\perp$ and $\mathbf{k}_\parallel$ dispersions, which and does not allow for a direct comparison with VLEED results. It should be noted that the non-FE behavior is much stronger for materials whose crystal potential is strongly modulated,

for example, for layered materials.[4,18,31]

Multiple coupling band composition of $E(k_\perp)$ can in fact severely impair the PE band mapping whichever method is used, as the final-state $k_\perp$ then becomes ambiguous. This composition does not necessarily result in multiple peaks in the PE spectra, because the peaks have a certain width determined by the final-state $k_\perp$ broadening $\mathrm{Im}\,k_\perp$, the initial-state energy broadening V_i^{hole}, their $k_\perp$ dispersions, and somewhat by the mode of data taking (see below). To simplify, resolving two PE peaks requires that (1) the $k_\perp$ separation of the final bands is larger than the sum of their $\mathrm{Im}\,k_\perp$; (2) the energy separation of the initial states due to their $k_\perp$ dispersion is larger than the sum of their V_i^{hole}. These conditions are met, for example, in the normal emission[12] from Cu(100) and some layered materials[4] which in certain final-state energy ranges demonstrate multiple spectral peaks. In other cases the multiple band composition results only in broadening and shifting of the PE peak because of averaging in $k_\perp$. This takes place, for example, in our cases shown in Fig. 6: the final bands are resolved in $k_\perp$ only marginally, and the available initial *d* bands are too flat.

To check the present experiment against multiple band effects, we investigated the whole dispersion region of E_{CFS} using the reference calculations. Only in the strong hybridization regions in Fig. 4, as expected, were the effects notable, but the main band from the $\Gamma KLUX$ plane still dominated in coupling. Only in the $\overline{\Gamma X}$ azimuth closer to the BZ border ($K_\parallel > 2$ Å^{-1}) did the additional bands acquire considerable coupling. Their small $k_\perp$ separation of (0.1–0.2)$|\Gamma X|$ from the main band and somewhat increased $\mathrm{Im}\,k_\perp$ suggest additional broadening and shifting of the PE peaks in this region, and thus less accurate band mapping (see below).

5. Effect of the surface relaxation

The Cu(110) surface is characterized by oscillatory relaxation: the first interlayer spacing is contracted by ~8.5%, and the second expanded by ~2.3% relative to the bulk value.[48] We have investigated its effect on the electronic structure by comparing VLEED data measured on different surfaces. Figure 9 shows two spectra reflecting $E(\mathbf{k})$ at the Γ point: one is measured on the (110) surface at $\mathbf{K}_\parallel = 2\overline{\Gamma Y}$ and the other on the almost unrelaxed (111) surface at normal incidence.[49] Their agreement is striking. For the Γ_2' and Γ_{15} points the dT/dE extrema differ in energy by less than 0.05 eV. For the Γ_{25}' point the difference reaches 0.2 eV, but this is because in the shown Cu(110) spectrum $K_\parallel$ increases by ~0.1 Å^{-1} at this energy; with the relevant spectrum the difference becomes less than 0.1 eV. A disagreement of the dT/dE peaks near 25 eV (by ~0.2 eV) is expected, as they correspond to different CP's displaced from the Γ point into the BZ interior along the ΓKX line and the ΓL line, respectively. The comparison thus suggests that the surface relaxation effect on the electronic structure is negligible.

B. Properties of the VLEED CFS PE method

1. Testing

As the first test of the VLEED-CFSPE method, we have checked the internal consistency of the experimental PE data.

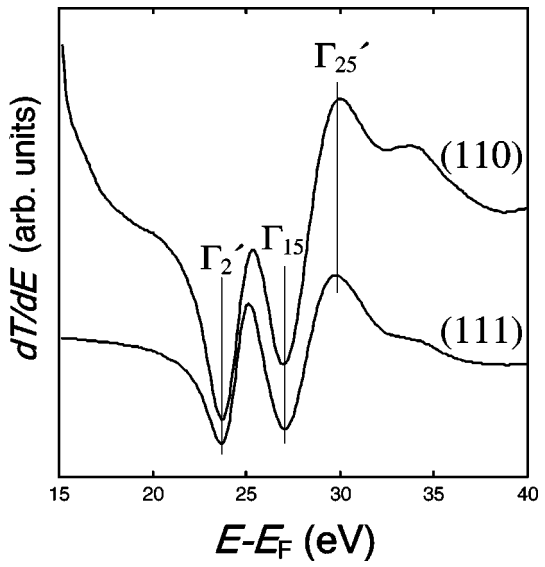

FIG. 9. Comparison of the VLEED data reflecting $E(\mathbf{k})$ at the Γ point: the spectrum measured on the relaxed Cu(110) surface at $\mathbf{K}_\parallel = 2\overline{\Gamma Y}$ (near $E = 25$ eV) and the one on the unrelaxed Cu(111) surface at normal incidence.

The band dispersions in Fig. 8 demonstrate excellent consistency not only in the *d* bands, but also, very convincingly, in the *sp* bands with their large $k_\perp$ dispersion. The dispersions remain smooth even where the final-state energies fall into the regions of strong band hybridization and undergo discontinuities (Fig. 4). As the most critical test, in a few such regions we measured a constant-$\mathbf{K}_\parallel$ series of CFS spectra, scanning the final-state energy through the discontinuity. Figure 10 shows a typical series. Although the intensity varies considerably due to variation of the matrix element

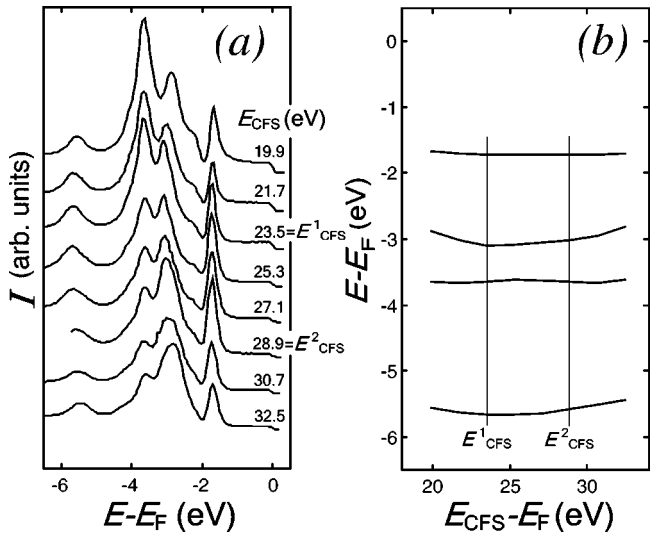

FIG. 10. A constant-$\mathbf{K}_\parallel$ series of CFS spectra (a) and the dispersion of the main peaks (b) on varying the final-state energy E_{CFS} through a E^1_{CFS}-to-E^2_{CFS} discontinuity of its dispersion determined by VLEED (Fig. 4) for $K_\parallel = 1.5$ Å^{-1} in the $\overline{\Gamma X}$ azimuth. The peak energies are almost constant through the discontinuity.

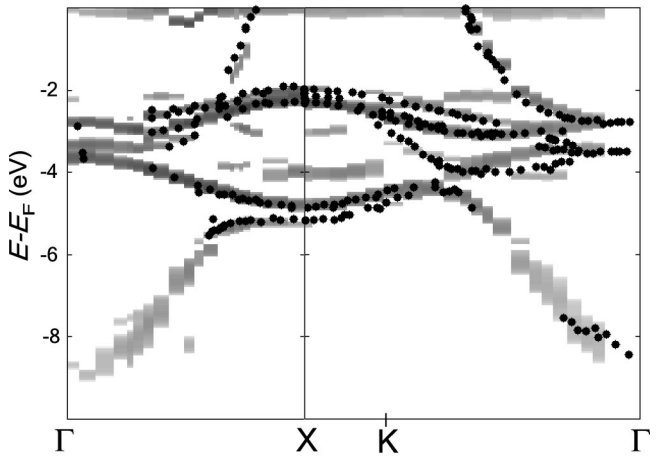

FIG. 11. Comparison of the VLEED-CFSPE valence band from Fig. 8 (in a lighter gray scale) with previous experimental data from different sources as compiled in Ref. 22. Note that the former shows all spectral structures, whereas the latter contain only the points interpreted as due to direct transitions, dropping the spurious structures like those due to 1DOS.

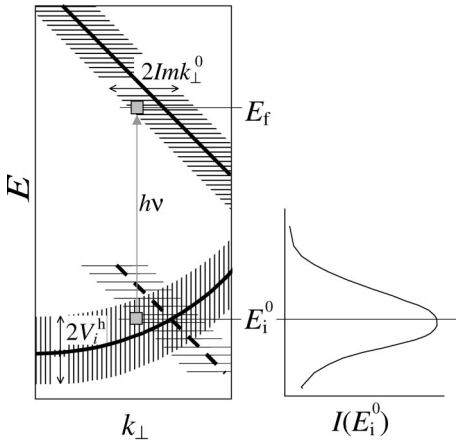

FIG. 12. Development of the PE peak profile due to the final-state $k_\perp$ broadening combined with the initial-state energy broadening. If the initial-state $k_\perp$ dispersion is nonlinear, the peak shifts somewhat toward larger numbers of the $dk_\perp$ states within the broadening overlap.

$|M_{fi}|^2$, the peak energies between the two E_{CFS} remain the same within ± 50 meV. Such small shifts may well be caused by, for example, the $|M_{fi}|^2$ variations within the peak profile. This behavior of the PE peaks confirms that the $k_\perp$ dispersion of the corresponding final-state band is nearly vertical through the whole region, as discussed above.

Second, the intentional choice of Cu has enabled us to test the method by comparing our results with a great deal of experimental data achieved by conventional methods.[20–23] Figure 11 shows our results compared with the representative points of virtually all available data sets as compiled in Ref. 22. Excellent correspondence is found in both positions and dispersions of the valence bands. The difference in covered pieces of the bands is due to different $|M_{fi}|^2$ connected with different final states. We stress that our data representation is most objective in showing *all* spectral structures, but the previous data are somewhat biased in showing only those interpreted as due to the direct transitions and deliberately dropping the minor structures like those due to 1DOS maxima, which, however can be found in the raw data.

Summarizing, our tests convincingly demonstrate that the combination of VLEED and CFSPE is a powerful and efficient method for absolute, i.e., truly **k**-resolving, band mapping of both the PE final and initial states. Fully automatic data processing has allowed for most unbiased testing.

2. New data on the valence band $E(\mathbf{k})$

Our experiment has provided new pieces of the valence band: (1) The sp band mapped along the whole ΓX line. The conventional mapping of this band on the (100) surface was troublesome due to the multiple band composition of the final state.[12,21] An additional problem was a very low intensity due to vanishing $|M_{fi}|^2$. Our method gains in intensity because the initial state is probed in a point of maximal 1DOS (see Fig. 1). The intensity gain has also enabled us to map the sp band along the ΓKX line almost to the Γ point; (2) $E(\mathbf{k})$ along the XL line. Its mapping inherently requires off-normal measurements, and is thus inaccessible by conventional band mapping. The VLEED-CFSPE method equally enables access to any oblique line in the surface-parallel symmetry planes.

A remarkable usefulness of the method should be stressed: very elegantly, one single PE experiment using one crystalline surface and one standard grating has covered almost the whole body of previous data and delivered new pieces of the Cu valence band.

3. Intrinsic accuracy

The intrinsic accuracy of the PE experiment is determined by certain shifts of the PE peaks from the true quasiparticle bands [i.e., the peaks of the spectral function $A(\omega,\mathbf{k})$]. Their roots lie in the finite electron and hole lifetimes. We here analyze the intrinsic accuracy effects connected with a *nonlinear* $k_\perp$ dispersion of the initial state, where the VLEED-CFSPE method is somewhat different from the conventional one. We remain within the bulk band structure picture.

We start with the mechanism of intrinsic broadening of the PE peaks (see, e.g., Refs. 2, 18, and 50). Briefly, the final state is characterized by a well-defined energy E_f and Lorentzian broadening in $k_\perp$, which is centered on $\mathrm{Re}\,k_\perp^0$ and has the HWHM $\mathrm{Im}\,k_\perp^0$. The initial state, complementarily, is characterized by a well-defined $k_\perp$ and broadening in energy, which is centered on the initial-state band $E_i(k_\perp)$ and whose HWHM is determined by the hole lifetime V_i^h (a common method of substituting this broadening by equivalent $k_\perp$ broadening[21,51] is restricted to a linear $k_\perp$ dispersion). As shown in Fig. 12, the photocurrent $I(E)$ occurs by adding up the elementary photocurrents from the direct transitions in all $dk_\perp$ states at the energy $E_i^0 = E_f - h\nu$, weighted by the above Lorentzians:

$$I(E_{\mathrm{i}}^0) \propto \int_{-\infty}^{+\infty} \frac{1}{(k_\perp - \mathrm{Re}\, k_\perp^0)^2 + (\mathrm{Im}\, k_\perp^0)^2} \times \frac{1}{[E_{\mathrm{i}}^0 - E_{\mathrm{i}}(k_\perp)]^2 + (V_i^{\mathrm{h}})^2}\, dk_\perp$$

(the spectral function normalization is dropped and the amplitude factors like $|M_{\mathrm{fi}}|^2$ are assumed constant).

If $E_{\mathrm{i}}(k_\perp)$ is nonlinear, the total number of $dk_\perp$ states within the broadening overlap relative to E_{i}^0 becomes different. Correspondingly, the PE peak becomes asymmetric, and its maximum experiences a certain intrinsic shift toward the larger number of states, deviating from the true band energy. In the band interior the peak will shift toward the band edge, where the 1DOS is larger. This effect is typical for conventional band mapping, in which the band dispersion is scanned in $k_\perp$. In the band extrema, on the contrary, the peak will shift toward the interior, as beyond the band limits there are no states (the effect of in-band shifting[4]). This situation is relevant for the VLEED-CFSPE method, in which the initial states are probed in the $E_{\mathrm{i}}(k_\perp)$ extrema. The intrinsic shifting effects are confirmed by one-step PE calculations.[52] They normally increase upon increase of the final- and initial-state broadening parameters.

The integral expression for the photocurrent can be evaluated analytically using the Taylor expansion of $E_{\mathrm{i}}(k_\perp)$. Here we will retain only the quadratic term $E_{\mathrm{i}}(k_\perp) = \alpha k_\perp^2$ (with an implicit V_{000} offset). At least near the band extrema used in the VLEED-CFSPE method this approximation suffices. The integrand then has three poles in the upper complex half plane:

$$\mathrm{Re}\, k_\perp^0 + i\, \mathrm{Im}\, k_\perp^0, \quad \sqrt{(E_{\mathrm{i}}^0 + iV_i^{\mathrm{h}})/\alpha},$$

and $-\sqrt{(E_{\mathrm{i}}^0 - iV_i^{\mathrm{h}})/\alpha}$. The corresponding residues form the three terms in $I(E_{\mathrm{i}}^0)$:

$$I(E_{\mathrm{i}}^0) \propto \frac{1}{\mathrm{Im}\, k_\perp^0} \frac{1}{(V_i^{\mathrm{h}})^2 + [E_{\mathrm{i}}^0 - \alpha(\mathrm{Re}\, k_\perp^0 + i\, \mathrm{Im}\, k_\perp^0)^2]^2} + \frac{1}{2\sqrt{\alpha} V_i^{\mathrm{h}}} \frac{1}{\sqrt{E_{\mathrm{i}}^0 + iV_i^{\mathrm{h}}}[(\mathrm{Im}\, k_\perp^0)^2 + (\sqrt{(E_{\mathrm{i}}^0 + iV_i^{\mathrm{h}})/\alpha} - \mathrm{Re}\, k_\perp^0)^2]}$$

$$+ \frac{1}{2\sqrt{\alpha} V_i^{\mathrm{h}}} \frac{1}{\sqrt{E_{\mathrm{i}}^0 - iV_i^{\mathrm{h}}}[(\mathrm{Im}\, k_\perp^0)^2 + (\sqrt{(E_{\mathrm{i}}^0 - iV_i^{\mathrm{h}})/\alpha} + \mathrm{Re}\, k_\perp^0)^2]}.$$

To compare the intrinsic accuracy of the VLEED-CFSPE and conventional methods, we performed model calculations using the above formalism. Their parameters corresponded to mapping of the *sp* band of Cu (for the *d* bands the intrinsic shifts are smaller due to their rather flat $k_\perp$ dispersion). The *sp* band was described by a FE quadratic dispersion, which is realistic far from the *d* bands. $\mathrm{Im}\, k_\perp$ was taken as ~ 0.12 Å^{-1}, which corresponds to our experiment at the Γ point (as determined by fitting the reference matching calculations including V_i to the corresponding VLEED spectrum; see above) and is representative in a wide range of the final-state energies. V_i^{h} was taken to vary linearly from zero at E_{F} to its value at the bottom of the *sp* band of ~ 0.9 eV (as determined by fitting the experimental PE peak width by this model calculation). The PE spectra were evaluated using the above analytical formula implying constant V_i^{h} within the peak profile. The calculations for the conventional band mapping assumed that the final-state $k_\perp$ dispersion is much larger than the initial-state one, which allowed us to neglect some $k_\perp$ variation within the peak profile in the EDC mode. It should be noted that in the conventional case these calculations are likely to underestimate the intrinsic shifts, as $\mathrm{Im}\, k_\perp$ is typically larger due to higher final-state energies.

The result of our modeling is shown in Fig. 13 as the position of the PE peaks on top of the true $E(\mathbf{k})$ (a) and the calculated intrinsic shifts (b). Remember that the VLEED-CFSPE method scans $E(\mathbf{k})$ in $\mathbf{k}_\parallel$, and the conventional one in $k_\perp$. On the whole, the two methods are characterized by comparable magnitude of the intrinsic shifting. There are, however, certain differences: (1) As expected, in the VLEED-CFSPE method the peaks are always slightly above the true band due to the in-band shifting in $E(k_\perp)$. In the conventional method the direction of shifting changes from in-band near the band bottom to opposite in the band interior; (2) The methods are entirely different near E_{F}, where V_i^{h} drops to zero: in the VLEED-CFSPE method the shifting also drops to zero, but in the conventional method it still remains. Indeed, as the first method probes the band in a $E(k_\perp)$ extremum, usually valleylike, there remain no occupied parts of the band upon crossing E_{F} and the PE peak shrinks into a singularity. In the second method there always remains an occupied part which within the $k_\perp$ broadening interval forms a certain width and thus an intrinsic shifting of the peak (in fact, upon crossing E_{F} the band always retain here a ghost peak; see, e.g. Refs. 52 and 53). This advantage of the VLEED-CFSPE method may be crucial for accurate mapping of the Fermi surface.

The values obtained of the intrinsic shifts based on real broadening parameters can in principle be immediately used to improve the accuracy of our experimental data (if far from the *d* bands).[25] At larger $\mathbf{k}$ along the ΓKX direction the intrinsic shifts somewhat increase due to larger $\mathrm{Im}\, k_\perp$ connected with the higher final-state energy.

It should be noted that our analysis neglects other sources of intrinsic shifting like variations of $|M_{\mathrm{fi}}|^2$ within the peak

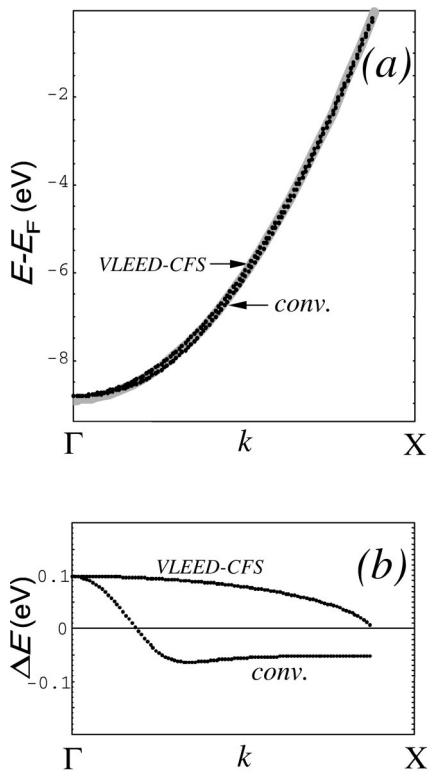

FIG. 13. Modeling of the intrinsic accuracy in the VLEED-CFSPE and conventional band mappings for the *sp* band of Cu: (a) the peak positions on top of the true $E(\mathbf{k})$ (thick gray line); (b) the intrinsic shifts.

profile[4] or smearing of the bulk 1DOS singularities near the surface. These effects can be taken into account within the explicit one-step theory of PE, but such calculations are much more difficult.[5,6,54]

In connection with the intrinsic accuracy it should be noted that the use of emission from final-state band gaps, a characteristic feature of the VLEED-CFSPE method, might seem a weakness compared to the conventional method: some enhancement of $\mathrm{Im}\,k_\perp$ in the gaps (Fig. 6) might result in an increase of the intrinsic shifting effects (and the 1DOS effects; see below). However, in practice the VLEED-CFSPE method is more accurate. This is because this enhancement of $\mathrm{Im}\,k_\perp$ is considerably smaller than the effect of V_i (Fig. 6 shows in fact a rare case of a rather large band gap combined with small V_i). This enhancement becomes important, as was most recently found for graphite, only if the band gap has an extraordinary width of the order of 10 eV.[55] As our method may be applied at low final-state energies, characterized by small V_i, on the whole $\mathrm{Im}\,k_\perp$ and thus the intrinsic accuracy limitations remain even smaller compared to the conventional method typically employing higher energies. In return, the accuracy of $\mathbf{k}$ along the direction of band mapping is free of the intrinsic broadening mechanisms, and limited only by the instrumental $\mathbf{k}_\parallel$ resolution (the latter also improves at low energies).

C. Valence band

The major peaks in the PE data in Fig. 8 all correspond to direct transitions from the bulk valence bands, as easily found from comparison to the band calculation. We will here concentrate, however, on the minor structures *A*–*F* which occur due to different mechanisms.

Structures due to the multiple band composition were expected, as discussed above, in the regions of strong upper band hybridization seen in the VLEED data. The shoulder-like structure *A* falls exactly in such a region, and its weakness reflects small coupling of the additional band (it would be helpful to confirm this interpretation against the 1DOS effects by varying E_{CFS} to check the $k_\perp$ dispersion). For large $\mathbf{k}$ along the ΓKX line the multiple coupling bands are close in $k_\perp$ to the main band, which results only in widening and shifting of the *sp* band peak to higher energies without resolving separate structures.

Some structures occur due to non-$k_\perp$-conserving transitions into 1DOS maxima away from the $\Gamma KLUX$ plane. Such structures were observed already in the $h\nu$-dependent normal emission spectra of Ref. 20. They are seen in our data as the shoulders *B* and *C*. The same effect is likely to form the shoulder *D*. Indeed, this structure is observed near $\mathbf{k}_\parallel = \overline{\Gamma X}$. By the symmetry of the bulk BZ the corresponding $E(k_\perp)$ should have band extrema, and thus 1DOS maxima, at the *X* point. The structure *D* is indeed close to the experimental energies of the *d* bands at this point and reflects their dispersion. This interpretation should again be checked against the $k_\perp$ dispersion.

The surface state structures may be distinguished from the 1DOS features by their smaller width. The peak *E* is a documented surface state.[22] The narrow shoulder *F* can be interpreted as a surface state or resonance split off the *d* states, not yet documented. This interpretation is corrborated by slab calculations on other surfaces.[56,57]

D. Excited-state self-energy effects

Comparison of the experimental valence band in Fig. 8 with a state-of-the-art DFT calculation, performed with the FLAPW code WIEN97,[35] reveals significant and systematic deviations: the experimental *d* bands are shifted by ~ 0.5 eV to lower energy, and the *sp* band in the opposite direction up to 0.4 eV (corrected for the intrinsic shifts) at the lowest point. These deviations are not due to any deficiencies of our experiment or band calculation, as the experimental results agree with the previous experimental data and the calculated $E(\mathbf{k})$ differs from any other modern calculation by less than 100 meV (the most recent analysis in Ref. 57 suggests that the early DFT calculations, showing a deceptive agreement with the experiment, are irrelevant due to technical flaws). Similar systematic deviations effects are found in the unoccupied bands.

The observed deviations manifest in fact the excited-state self-energy corrections $\mathrm{Re}\,\Delta\Sigma$ to the ground-state DFT eigenvalues, surprisingly large in spite of the less correlated nature of Cu. These effects are discussed in detail in Ref. 25. Briefly, the distinct band dependence of $\mathrm{Re}\,\Delta\Sigma$ is related to a different spatial localization of the one-electron wave functions. For example, the valence *d* electrons are localized in the core region with large electron density $n(\mathbf{r})$, and thus experience a larger effective density n_{eff} as compared to the

sp electrons delocalized over the unit cell. This gives rise to a difference in the self-energy effects[58] largely determined by n_{eff}. Qualitatively, these effects can be mapped onto the electron gas exchange-correlation behavior through generalization of n_{eff} as a wave function weighted density $\int_\Omega \phi^*_{\mathbf{k}}(\mathbf{r})\phi_{\mathbf{k}}(\mathbf{r})n(\mathbf{r})d\mathbf{r}$ with integration over the unit cell. An explicit description of the excited-state exchange and correlation in the framework of the GW approximation provides a good quantitative description of the observed band dependence of $\mathrm{Re}\,\Delta\Sigma$.[25]

V. CONCLUSION

A method for absolute band mapping with full control of the three-dimensional **k**, the VLEED-CFSPE method, has been described in detail. The method is based on determination of the final-state band gap dispersions along the surface-parallel symmetry lines of the BZ using angle-dependent VLEED measurements. The corresponding final-state energies are then used to map the valence band $E(\mathbf{k})$ using PE measurements in the CFS mode.

The main advantage of the VLEED-CFSPE method is a natural incorporation of the non-FE and excited-state effects in the upper bands, which delivers an accuracy superior to that of conventional techniques. The method can thus be applied in conventionally troublesome situations like materials with strong modulation of the crystal potential or the low-$h\nu$ region, attractive for the best **k** resolution. The method has further advantages: (1) a PE intensity gain by virtue of measuring initial states at maximal 1DOS; (2) better intrinsic accuracy near E_{F}; (3) practical utility in that use of a narrow $h\nu$ range and only one crystal surface allows for complete band mapping along a variety of BZ directions. For many crystals having only one stable surface, for example, layered materials, this method is the only possibility for determining $E(\mathbf{k})$ in a thorough and well-characterized way. It should be noted, however, that the VLEED-CFSPE method, providing control over the three-dimensional **k**, employs more elaborate data analysis and data acquisition techniques compared to conventional band mapping.

Applying the VLEED-CFSPE method to Cu, we have mapped the surface-projected dispersions of unoccupied bands and explicitly determined the strength of their non-FE behavior. Contrary to common belief, such behavior is significant in extended regions of **k** space. Through the upper and valence bands we have also found significant deviations from the DFT picture. This reveals significant self-energy effects in Cu despite its less correlated nature.

ACKNOWLEDGMENTS

We gratefully acknowledge financial support by the Deutsche Forschungsgemeinschaft and Chalmers University of Technology.

*Also at the Institute for High-Performance Computations and Data Bases, P. O. Box 71, 194291 St. Petersburg, Russia.

[1] *Angle-Resolved Photoemission*, edited by S. D. Kevan (Elsevier, Amsterdam, 1992).

[2] S. Hüfner, *Photoelectron Spectroscopy* (Springer, Berlin, 1995).

[3] P. O. Nilsson and N. Dahlback, Solid State Commun. **29**, 303 (1979); P. Heinman, M. Miosaga, and H. Neddermeyer, *ibid.* **29**, 467 (1979).

[4] V. N. Strocov, H. Starnberg, P. O. Nilsson, H. E. Brauer, and L. J. Holleboom, Phys. Rev. Lett. **79**, 467 (1997); J. Phys.: Condens. Matter **10**, 5749 (1998).

[5] P. J. Feibelman and D. E. Eastman, Phys. Rev. B **10**, 4932 (1974).

[6] J. B. Pendry, Surf. Sci. **57**, 679 (1976).

[7] G. Capart, Surf. Sci. **13**, 361 (1969).

[8] J. B. Pendry, J. Phys. C **2**, 2273 (1969).

[9] J. B. Pendry, *Low Energy Electron Diffraction* (Academic Press, London, 1974).

[10] R. C. Jaklevic and R. C. Davis, Phys. Rev. B **26**, 5391 (1982).

[11] V. N. Strocov, H. Starnberg, and P. O. Nilsson, J. Phys.: Condens. Matter **8**, 7539 (1996).

[12] V. N. Strocov, H. Starnberg, and P. O. Nilsson, Phys. Rev. B **56**, 1717 (1997). An experiment on Cu(100) using an improved setup (Ref. 29) has corrected the position of the lower band of the doublet: it crosses the Γ point near 26.5 eV.

[13] V. N. Strocov, Solid State Commun. **106**, 101 (1997).

[14] On a qualitative level, the coupling bands may be identified as having a large partial content of the coupling Fourier components which resemble the incident plane wave (see, e.g., Ref. 10). These components are most conveniently identified through equivalence of the surface-parallel wave vectors $\mathbf{k}_\parallel + \mathbf{G}_\parallel = \mathbf{K}_\parallel$ and codirection of the surface-perpendicular ones $(k_\perp + G_\perp)/K_\perp > 0$ (Refs. 13 and 15). To this end it should be noted that in PE only the second condition is often used to model the surface transmission (Ref. 40), its insufficiency becomes obvious, for example, from matching calculations in the empty-lattice limit.

[15] V. N. Strocov, Solid State Commun. **78**, 545 (1991); Int. J. Mod. Phys. B **9**, 1755 (1995).

[16] V. N. Strocov, Int. J. Mod. Phys. B **7**, 2813 (1993).

[17] Relevance of the sudden approximation can be assessed from the electron-hole interaction energy as found by comparison of the VLEED and PE data on a few characteristic points in the upper bands (Ref. 4). In all known cases this energy is negligible.

[18] V. N. Strocov, in *Electron Spectroscopies Applied to Low-Dimensional Materials* (Kluwer, Dordrecht, 2000).

[19] R. Courths, H. Wern, G. Leschik, and S. Hüfner, Z. Phys. B: Condens. Matter **74**, 233 (1989).

[20] P. Thiry, Ph.D. thesis, University of Paris, 1979; Y. Petroff and P. Thiry, Appl. Opt. **19**, 3957 (1980).

[21] J. A. Knapp, F. J. Himpsel, and D. E. Eastman, Phys. Rev. B **19**, 4952 (1979).

[22] R. Courths and S. Hüfner, Phys. Rep. **112**, 53 (1984).

[23] R. Matzdorf, Surf. Sci. Rep. **30**, 153 (1998).

[24] V. N. Strocov, R. Claessen, G. Nicolay, S. Hüfner, A. Kimura, A. Harasawa, S. Shin, A. Kakizaki, H. I. Starnberg, P. O. Nilsson, and P. Blaha, Phys. Rev. Lett. **81**, 4943 (1998).

[25] V. N. Strocov, F. Aryasetiawan, P. O. Nilsson, P. Blaha, G. Nicolay, S. Hüfner, and R. Claessen (unpublished).

[26] G. Capart, Surf. Sci. **26**, 429 (1971).

[27] V. Heinrich, Rev. Sci. Instrum. **44**, 456 (1973).
[28] S. A. Komolov, *Total Current Spectroscopy of Surfaces* (Gordon and Breach, Philadelphia, 1992).
[29] V. N. Strocov, Meas. Sci. Technol. **7**, 1636 (1996).
[30] A slight shoulder near 25 eV close to $K_{\|}=0$ was found to build up its intensity gradually within $\sim$15 min after annealing of the sample. Not connected with $E(\mathbf{k})$, it may originate from diffusion of impurities (presumably sulfur) from the bulk.
[31] V. N. Strocov, P. Blaha, H. I. Starnberg, M. Rohlfing, R. Claessen, J.-M. Debever, and J.-M. Themlin, Phys. Rev. B **61**, 4994 (2000).
[32] D. L. Smith and C. Mailhiot, Rev. Mod. Phys. **62**, 173 (1990).
[33] E. E. Krasovskii and W. Schattke, Phys. Rev. B **56**, 12 874 (1997).
[34] G. Nicolay *et al.* (unpublished).
[35] P. Blaha, K. Schwarz, and J. Luitz, WIEN97, Vienna University of Technology, 1997 [Improved version of P. Blaha, K. Schwarz, P. Sorantin, and S. B. Trickey, Comput. Phys. Commun. **59**, 339 (1990)].
[36] Yu. P. Chuburin, G. V. Wolf, D. V. Fedorov, and V. N. Strocov, Fiz. Tverd. Tela (St. Petersburg) **41**, 2105 (1999); [Phys. Solid State **41**, 2105 (1999)].
[37] Only in the region of $K_{\|} > 2$ Å^{-1} in the $\overline{\Gamma X}$ azimuth was the interpretation unsure. Here $E(\mathbf{k})$ near the $\Gamma KLUX$ plane is characterized by a multitude of hybridizing bands with close coupling properties, which is reflected by multiple weak and hardly resolvable structures in the VLEED spectra (Fig. 3). In this region we verified our interpretation by taking few fast CFS spectra and checking the extremal behavior of the valence *sp* band under variation of E_{CFS}.
[38] A. Goldmann, W. Altmann, and V. Dose, Solid State Commun. **79**, 511 (1991).
[39] The spectrum in the $\overline{\Gamma Y}$ azimuth closest to the Γ point was by mistake taken with E_{CFS} in the band gap below the E_{CFS} dispersion discontinuity (see Fig. 4). This, however, should only slightly affect the PE spectra because of rather vertical $E(k_{\perp})$ of the final bands in this region.
[40] H. Przybylski, A. Baalmann, G. Borstel, and M. Neumann, Phys. Rev. B **27**, 6669 (1983).
[41] S. C. Wu, J. Sokolov, C. K. C. Lok, J. Quinn, Y. S. Li, D. Tian, and F. Jona, Phys. Rev. B **39**, 12 891 (1989).
[42] E. G. McRae, Rev. Mod. Phys. **51**, 541 (1979).
[43] R. O. Jones and P. J. Jennings, Surf. Sci. Rep. **9**, 165 (1988).
[44] P. O. Nilsson, K. Karlsson, and J. Rundgren, Phys. Rev. B **47**, 12 968 (1993).
[45] M. Graß, J. Braun, G. Borstel, R. Schneider, H. Dürr, Th. Fauster, and V. Dose, J. Phys.: Condens. Matter **5**, 599 (1993).
[46] A. Baalmann, M. Neumann, W. Braun, and W. Radlik, Solid State Commun **54**, 583 (1985). Their method was based on mapping of the valence band CP's along a symmetry line that is *not* parallel to the surface, which makes unambiguous location of these points in **k** space difficult.
[47] A. P. J. Stampfl, J. A. Con Foo, R. C. G. Leckey, J. D. Riley, R. Denecke, and L. Ley, Surf. Sci. **331-333**, 1272 (1995).
[48] I. Stensgaard, R. Feidenhans'l, and J. E. Sørensen, Surf. Sci. **128**, 281 (1983); D. L. Adams, H. B. Nielsen, and J. N. Andersen, *ibid.* **128**, 294 (1983).
[49] V. N. Strocov and H. I. Starnberg (unpublished).
[50] R. Matzdorf, Appl. Phys. A: Mater. Sci. Process. **63**, 549 (1996).
[51] N. V. Smith, P. Thiry, and Y. Petroff, Phys. Rev. B **47**, 15 476 (1993).
[52] K. W.-K. Shung and G. D. Mahan, Phys. Rev. Lett. **57**, 1076 (1986).
[53] E. Jensen and E. W. Plummer, Phys. Rev. Lett. **55**, 1912 (1985).
[54] E. Pehlke, W. Schattke, O. Anderson, R. Manzke, and M. Skibowski, Phys. Rev. B **41**, 2982 (1990).
[55] V. N. Strocov, A. Charrier, J.-M. Themlin, M. Rohlfing, R. Claessen, N. Barrett, J. Avila, J. Sanchez, and M.-C. Ascensio, Phys. Rev. B (to be published).
[56] Y. Yang, S. C. Wu, F. Q. Liu, K. Ibrahim, H. I. Qian, S. H. Lu, and F. Jona, Phys. Rev. B **54**, 5092 (1996).
[57] R. Courths, M. Lau, T. Scheunemann, H. Gollisch, and R. Feder, Phys. Rev. B (to be published).
[58] P. O. Nilsson and C. G. Larsson, Phys. Rev. B **27**, 6143 (1983).